

# A 4D treatment planning system for scanned ion beam therapy

D. Richter<sup>1,2</sup>, A. Schwarzkopf<sup>1,2</sup>, J. Trautmann<sup>1,2</sup>, M. Krämer<sup>1</sup> (?), M. Durante<sup>1,2</sup>, O. Jäkel<sup>3</sup>, C. Bert<sup>1,3</sup>

<sup>1</sup>GSI Helmholtzzentrum für Schwerionenforschung GmbH, Abt. Biophysik, Planckstraße 1, 64291 Darmstadt, Germany

<sup>2</sup>TU Darmstadt, Hochschulstraße 6, 64289 Darmstadt, Germany

<sup>3</sup>University Heidelberg, Clinic for Radiation Oncology, Im Neuenheimer Feld, Heidelberg

## I. Abstract

**Purpose:** To develop a research 4D treatment planning system (4DTPS) suitable for realistic patient treatment planning and treatment simulations taking into account specific requirements for scanned ion beam therapy, i.e. modeling of dose heterogeneities due to interplay effects and range changes caused by patient motion and dynamic beam delivery.

**Methods:** The 4DTPS integrates interfaces to data of 4D computed tomography (4DCT), deformable image registration and clinically used motion monitoring devices. We implemented a novel data model for 4D image segmentation using Boolean mask volume datasets and developed an algorithm propagating a manually contoured reference contour dataset to all 4DCT phases. We further included detailed treatment simulation and dose reconstruction functionality, based on the irregular patient motion and the temporal structure of the beam delivery. The treatment simulation functionality was validated against experimental data from irradiation of moving radiographic films in air, 3D moving ionization chambers in a water phantom and moving cells in a biological phantom with a scanned carbon ion beam. The performance of the program was compared to results obtained with predecessor programs.

**Results:** The measured optical density distributions of the radiographic films were reproduced by the simulations to on average about  $(-2 \pm 12) \%$ . Compared to the predecessor program, the mean agreement was on average improved by 2 %, standard deviations were on average reduced by 7 %. The simulated dose to the moving ionization chambers in water showed an agreement with the measured dose of on average  $(-1 \pm 4) \%$  for the typical beam configuration. The mean average deviation of the simulated from the measured biologically effective dose determined via the cell survival was  $(617 \pm 538) \text{ mGy (RBE)} (10 \pm 9) \%$ .

**Conclusion:** We developed a research 4DTPS suitable for realistic treatment planning on patient data and capable of simulating dose delivery to a moving patient geometry for scanned ion beams. With respect to the predecessor program, the accuracy and reliability of treatment simulations could be considerably improved.

## 35 II. Introduction

Treatment planning for radiotherapy incorporating the time domain is typically referred to as 4D treatment planning.<sup>1</sup> It has been investigated in parallel to the development of 4D computed tomography (4DCT). Several reviews have been published in that field.<sup>2-4</sup>

40 In this report we focus on 4D treatment planning for ion beam therapy that has to incorporate range changes due to target motion into the treatment concept. Since treatments of tumors in the vicinity of moving organs are delivered since many years with either proton or ion beams, also treatment planning concepts have been established. For treatment of lung tumors at the National Institute for Radiological Sciences (NIRS), gating is used<sup>5</sup> and treatment planning ensures by manual manipulation of the CT that the tumor mass is elongated in the superior-inferior (SI) direction to avoid under-dosage at the distal end if less dense lung tissue is replaced by dense tumor due to breathing.<sup>6</sup> With the availability of 4DCTs 45 this approach has been developed. Engelsman *et al.* compared three treatment planning strategies for lung tumor treatment by a scattered proton beam with margins only.<sup>7</sup> Based on the 4DCT of the patient they designed the shape of compensator and aperture and found better coverage of the clinical target volume (CTV) with these treatment plans compared to conventional ones. Similar work has been 50 reported by Kang *et al.* as well as Mori *et al.*, who designed a complete 4D treatment planning system (4DTPS) including visualization of range changes due to target motion (called ‘Aqualyzer’).<sup>8-10</sup>

If treatments are delivered with a scanned beam, interplay effects pose an additional challenge also for the 4DTPS.<sup>11,12</sup> Optimization of treatment plans has to consider the specific parameters of the used motion mitigation technique, e.g., the number of rescans, or the calculation of compensation parameters 55 for beam tracking. 4D dose calculation has to incorporate the temporal progress of the beam delivery and to establish a correlation to the motion states of the 4DCT. Several groups report about 4D dose calculation for beam scanning. The Paul Scherrer Institute (PSI) plans to irradiate intra-fractionally moving tumors with rescanning and thus oriented their 4DTPS-based studies in this direction.<sup>13-16</sup> They currently use 4DCTs as the basis of 4D dose calculation but consider to incorporate 4D magnetic resonance tomograms (4DMRT) to exploit the possibilities of long acquisition times that allow to 60 determine potential changes in the motion trace. Also Kraus *et al.* investigated rescanning for scanned proton beam therapy in 4D treatment planning studies.<sup>17</sup> Paganetti *et al.* published several reports on 4D treatment planning for proton beam therapy with scanned as well as scattered beams.<sup>18,19</sup> More details on 4DTPS can be found in a review<sup>20</sup> and in the introduction of each of the following sections in the 65 Materials & Methods.

This work focuses on the GSI TPS “Treatment planning for Particles” (*TRiP98*) that was developed by Krämer *et al.* for the GSI pilot project<sup>21-23</sup> and which evolved into a 4DTPS in the last decade. Initial attempts made at GSI with respect to irradiation of moving tumors were focused on the implementation of a beam tracking solution. Li *et al.* established a simulation environment based on *TRiP98* 70 concentrating on 4D dose calculation for beam tracking and uncompensated irradiation of rigidly moving targets.<sup>24</sup> The program was capable of 4D dose calculation for artificial and experimental water phantom setups with variable time resolution<sup>25</sup> but not compatible with the upcoming 4DCT and deformable registration workflows as developed in parallel to 4DCT.<sup>1,26</sup> The new workflow was the basis of the following implementation of Bert & Rietzel.<sup>27</sup> The temporal changes of the anatomy during 75 beam delivery, i.e. the transitions through the CT phases, were determined from motion monitoring traces. Sub-treatment plans for each 4DCT phase, containing all raster points irradiated in a particular phase, were generated on the basis of the time-correlated motion trace and a time-resolved beam delivery sequence. 4D physical dose calculation was established by sequential 3D dose calculation for each sub-treatment plan on the respective CT phases and subsequent transformation of the sub-distributions to the reference phase. Apart from beam tracking and uncompensated irradiation, the 80 program also was capable of simulating rescanned and gated beam delivery techniques. Compared to Li *et al.* the time structure of the irradiation was incorporated in a more realistic way using beam intensity courses simulated or measured over the entire delivery time. Moreover, 4D optimization functionality was developed comprising the calculation of motion compensation parameters for beam tracking and the design of internal target volumes (ITV) in water-equivalent space for realistic patient geometries. An improved version of beam tracking takes into account real-time adaption of the particle numbers per 85 raster point, in order to compensate for dose changes caused by target rotation or deformation.<sup>28</sup> Validation of the 4DTPS was performed in numerous experiments.<sup>29</sup>

90 The sequential nature of the TPS and the 4D dose calculation algorithm developed by Bert & Rietzel has  
proven incompatible with biologically effective dose calculation. Since the relative biological  
effectiveness (RBE) depends non-linearly on the full spectrum of energies and particles contributing to  
the total physical dose at each point in the treatment field, it cannot be determined from the constituent  
physical dose distributions per CT phase. Therefore, Gemmel *et al.* developed a complementary 4D dose  
95 calculation algorithm. It featured a dedicated 4DCT structure for full access during run-time and a new  
biological dose calculation concept considering particle spectra and dose contributions from all CT  
phases to the total dose at each point in the treatment field. The code has been successfully verified in  
cell survival measurements in the presence of target motion.<sup>30</sup>

100 Although well tested and established in experiments, the 4DTPS codes previously available at GSI carry  
substantial limitations with respect to 4D treatment planning for realistic patient geometries, especially if  
embedded in a clinical workflow. Among the necessities requiring re-implementation and further  
development of our 4DTPS (TRiP4D) based on TRiP98 were: Handling of 4D structure sets,  
incorporation of motion monitoring data from clinically used systems, robust import of the scanning  
progress data, flexible use of deformation maps, compatibility to future developments such as 4D  
105 treatment plan optimization of multiple fields, and validation based on complex measurements with  
precise ionization chambers.

The following sections will report these developments embedded in a review of existing solutions in the  
literature as well as in previous versions developed at GSI.

### III. Material and Methods

110 In the following, the implementation of the 4D treatment planning functionality of *TRiP4D* will be  
discussed. The first section will concentrate on modeling of patient anatomy changes. Subsequently, the  
currently pursued 4D optimization strategy will be discussed. In the last section *TRiP4D*'s 4D treatment  
simulation capabilities and the required components are dealt with.

#### III. A. Moving patient geometry

115 Imaging, characterization and quantification of the moving patient geometry can be considered the first  
step in 4DTP.<sup>1,3</sup> Time-resolved computed tomography (4DCT) has proven essential for the assessment  
of patient motion and 4D treatment planning tasks, such as the design of safety margins and 4D dose  
calculation.<sup>26</sup> Dedicated 4DCT structures and functionality have been implemented in *TRiP4D*, allowing  
access to all motion states of the 4DCT in parallel in order to fully exploit its potential for treatment  
planning. The program makes use of the VOXELPLAN format for any data input and output.<sup>31</sup> The  
120 usability of DICOM standard CT data is guaranteed by dedicated in-house DICOM converter software.

##### III. A. 1. Motion monitoring data

125 For simulation of a 4D treatment delivery, the transition of the patient through the 4DCT states over  
time has to be known. Signal handling and processing of realistic patient motion trajectories has been  
integrated into *TRiP4D*. Apart from a general purpose interface, compatibility of the TPS to the ANZAI  
AZ-733 system (ANZAI Medical Co., Ltd.) has been established providing a one-dimensional surrogate  
signal from either a pressure sensor in a waist belt or a laser distance measurement. For simulation  
studies, dedicated routines are available for automatic generation of regular sinusoidal motion traces or  
traces according to Lujan *et al.*<sup>32</sup>

130 To allow dosimetric assessment of, e.g., baseline drifts or phase shifts between tumor motion and  
motion surrogate, two different kinds of motion signals can be used in parallel, i.e. the surrogate signal  
and the internal motion signal. The latter holds the *true* motion data to be used for 4D dose calculation.  
The former represents the *observed* motion signal which is, e.g., used to control beam gating or select  
beam tracking parameters.

##### III. A. 2. Image registration and deformation maps

135 Quantification of the implicit information of 4DCT data, i.e. the spatial and temporal changes of the  
patient's anatomy, can be achieved with image registration which establishes the alignment between a  
fixed reference state CT and a test 4DCT state. The resulting deformation maps represent voxel-to-voxel  
displacements between the reference motion state and each other motion state of the 4DCT. Various

140 algorithms have been published in the literature.<sup>33-35</sup> *TRiP4D* does not (yet) include native image registration functionality. To allow incorporation of data from established registration tools, we implemented a filter that allows the use of deformation maps in volume dataset representation featuring one CT-like structure per displacement vector component and state transition. This representation is compatible with registration output of many available tools, including the code Plastimatch<sup>36</sup> that we currently use. Additionally, *TRiP4D* supports rigid registration employing the commonly used  $4 \times 4$  matrix representation and formalism.<sup>37</sup>

To conveniently assess the extent and distribution of patient motion on the basis of the available deformation maps, motion volume histograms (MVHs) and contour-based export of the 3D motion amplitude have been implemented. Figure 1 illustrates the functionality in the example of a liver tumor and the displacement field between the end-exhale and end-inhale 4DCT phases.

### 150 III. A. 3. 4D segmentation

Elaborate 4D treatment planning requires information on the spatial and temporal changes of target volumes and organs at risk. Manual contouring on all 4DCT states by a physician is time-consuming and in general not feasible in a clinical workflow. Automatic propagation of manually delineated reference contours is a promising and efficient approach to obtain contours on all 4DCT states.<sup>38,39</sup> The design of ITVs and other steps in the 4DTP workflow can benefit from full integration of 4D segmentation into the treatment planning system. Therefore, *TRiP4D*'s existing module for handling 3D segmentation has been enhanced with respect to 4D treatment planning functionality. This comprises a novel 4D contour data model, a contour propagation algorithm and contour manipulation functionality.

160 The segmentation module of *TRiP98* relies on VOXELPLAN contour data given in the form of coplanar polygons usually originating from manual delineation on axial CT slices. The new implementation of 4D segmentation extends the 3D functionality by the integration of volumetric Boolean masks (VBMs), i.e. a representation of 4DVOIs as Boolean masks held in a volume dataset structure. This approach is based on several arguments. Firstly, a major focus was on the design of an integrated 4D structure capable of handling VOIs in all CT states. Flexible combination of individual volumes should also be supported and is particularly simple in the approach of VBMs. Secondly, volume datasets are well established structures in *TRiP4D* and existing functionality can be re-used efficiently. And thirdly, contour propagation involves deformation of VOIs. In this context VBMs offer advantages over polygonal contours.

170 For generation of a VBM, each voxel center is tested for its position with respect to the polygon VOI. A point-in-polygon ray-casting algorithm based on the Jordan curve theorem is used to determine whether the respective voxel is inside the polygon VOI.<sup>40,41</sup> Voxels inside the polygon VOI are marked in the volume dataset using a bit mask. A single bit per VOI representation and voxel is required. Consequently, different VOI motion states can be held on individual bits in a single volume dataset. Figure 2a illustrates the conversion of a polygon contour into a VBM and the resulting bit patterns for the different VOI states. In order to ensure compatibility with other software packages, e.g., external visualization tools, VBM datasets can be re-converted into polygon contours. Contour detection routines have been implemented based on a Freeman code chain algorithm.<sup>42</sup> The enveloping polygons of the VOI volume are reconstructed in each axial slice of the volume dataset (dashed lines in Figure 2a) taking into account potential separation of sub-VOIs. Further manipulation of the 4DVOI can be performed conveniently using the VBM datasets. For instance, formation of geometrical unions or intersections among different VOI states involves bit mask operations only and has been implemented in *TRiP4D* for further 4DTP tasks.

185 Different methods of contour propagation have been published in the literature and are commonly divided into deformable registration-based<sup>38,43,44</sup> and deformable model-based<sup>45,46</sup> methods. Contour propagation in *TRiP4D* employs a deformable registration-based approach taking advantage of the already discussed infrastructure for deformable registration maps. The underlying concept is to guide the transformation of the reference state VOI with the deformation fields obtained from registration of the underlying CT geometry. The use of coplanar polygons alone poses problems in contour propagation, since the coplanar character is in general lost under spatial transformation. For this reason, triangular mesh surfaces are used by some groups to model transformation of the VOI.<sup>38,47</sup>

190

*TRiP4D* follows an alternative approach employing VBM dataset structures for contour propagation from the reference state  $r$  to all states  $i \neq r$ . Let  $\vec{q}_{l,m,n} = (x_l, y_m, z_n)$  denote the position of the voxel centers. Propagation of the reference state VOI to state  $i$  is performed by inverse transformation of each voxel center  $\vec{q}_{l,m,n}$  to the reference state  $\vec{p} = \vec{q}_{l,m,n} + \vec{u}_{i,r}(\vec{q}_{l,m,n})$ . Here,  $\vec{p}$  denotes the reference state position of  $\vec{q}_{l,m,n}$ . The displacement vectors,  $\vec{u}_{i,r}$ , are obtained from the inverse deformation maps as discussed earlier in this section. The position of  $\vec{p}$  with respect to the reference state contour is tested using the point-in-polygon ray-casting algorithm described earlier. Voxel positions having a source point inside the polygonal reference contour are marked in the volume dataset as a VBM using separate bits for different states. It should be noted that the described propagation algorithm does not require transformation of the VBM in the reference state. Instead, it makes direct use of the (physician-approved) polygonal reference state contour to obtain the VBM-VOIs in all states.

### III. B. 4D treatment plan optimization strategy

Depending on the employed motion mitigation technique, different strategies have to be used for 4D treatment plan generation. *TRiP4D* allows generation of internal target volumes<sup>48</sup>, i.e. unions of CTVs that incorporate range changes caused by organ motion. Such ITVs are required for motion mitigation techniques that compensate dosimetric effects of interplay but not the target motion itself. The most prominent example of such a technique is rescanning. Several versions of these range-change-proof ITVs have been pursued in the last years. Details can be found in the literature.<sup>27;49;50</sup>

As an additional 4D optimization technique, the calculation of motion compensation parameters for beam tracking is supported. In beam tracking the beam position is adjusted to the tumor motion in real-time.<sup>25</sup> During beam delivery, pre-calculated correction vectors are applied to the planned beam position according to the current motion state of the patient.<sup>27</sup> A more elaborate version of beam tracking, real-time dose compensated beam tracking (RDBT), additionally compensates for potential dose changes of tumor areas with respect to the reference treatment plan.<sup>28</sup> Both techniques have been published previously and the functionality is available in *TRiP4D*.

### III. C. Simulation of 4D treatment delivery

Dose deposition for moving targets in scanned ion beam therapy is determined by the double-dynamic nature of the system representing the origin of the interplay effect. Firstly, the beam delivery process itself is time-dependent, since the beam is scanned over the target. Secondly, the effective beam position is affected by target motion. Both contributing aspects have to be modeled adequately in the TPS, in order to enable simulation of 4D treatments. It has been shown with earlier versions of the GSI 4DTPS that simulation of dose delivery subsequent to treatment is well feasible for experimental setups.<sup>24;29;30</sup>

*TRiP4D* has been extended for simulation of clinical 4D treatment delivery in realistic patient environments. This particularly includes irregular surrogate motion trajectories, 4D dose calculation using transformation maps obtained from deformable image registration and time-resolved beam delivery sequence data compatible with clinically used accelerators, e.g., HIT. In the following sections the integration of clinical motion monitoring data and the time structure of the beam delivery process into *TRiP4D* are described. Temporal correlation of these two components finally enables simulation of physical and biological 4D dose deposition which considers the specific motion characteristics at treatment delivery time. The implementation of these aspects will be discussed in the last subsection.

#### III. C. 1. Motion state identification

In section II. A. 1 the principal incorporation of motion monitoring data into *TRiP4D* was discussed. Simulation of 4D treatments in *TRiP4D* requires information on the transition of the patient through the 4DCT phases over time. Surrogate motion monitoring data acquired concurrently to beam delivery can provide this information, given that the identification of the motion state is performed in agreement with the 4DCT reconstruction process.<sup>51;52</sup>

Motion state identification is a central functionality of *TRiP4D*'s motion trajectory module. Different methods are available based on: (i) the absolute signal amplitude, (ii) the signal phase and (iii) the relative signal amplitude. The latter is needed in particular for use in conjunction with the ANZAI system. In contrast to amplitude-based motion state identification, the methods (ii)-(iii) require dedicated signal pre-processing prior to motion state identification. For phase-based identification, the signal phase

is computed using the Hilbert transform of the original signal.<sup>53</sup> The Hilbert transform is obtained by external fast Fourier transform routines.<sup>54</sup> For relative-amplitude based identification as it is, e.g., used in some Siemens 4DCT scanners, the original signal is converted into a normalized trajectory with a fixed amplitude range. This is done based on a search for the maximum and minimum position in each respiratory cycle and subsequent normalization of the signal to the amplitude range in each exhale (negative slope) and inhale branch, respectively.

### III. C. 2. Beam delivery sequence and time structure

In raster scanning, the individual dwell time per raster point depends on the requested particle fluence and the intensity delivered by the accelerator. Due to the complexity of the system, a priori modeling of the time structure of beam delivery is challenging, especially if beam pauses caused by gating or by the synchrotron are to be considered. However, the time structure, called beam delivery sequence (BDS) in the following, can be measured during irradiation. The procedure to obtain the BDS can be considered highly facility dependent. Nevertheless, several general beam delivery events (BDE) can be expected to be accessible at any scanning facility. Table 1 summarizes the types of BDE and the possible transitions between them.

*TRiP4D* provides the interface to a generally defined table format for BDS input files describing the chronology of BDE. The tables have to be compiled externally according to the specific conditions of the respective machine. Data source can be an already delivered treatment or a simulation of such.

### III. C. 3. 4D dose deposition

4D dose deposition is fully determined by the treatment plan, the time structure of the beam delivery and the patient motion. In order to account for dose contributions to each dose voxel in consideration of target motion, knowledge is required on which raster points were fully or partly irradiated in a certain motion state. This information is obtained from the combined time courses of the BDS and the surrogate motion trajectory. Since the treatment control system and the motion monitoring device are usually independent medical products of different manufacturers, beam delivery and motion monitoring naturally do not share the same data acquisition and system time. Prior importing the data into *TRiP4D*, external software has to be used to temporally align the traces, e.g., based on BON or BOF BDE (see Table 1).

Temporal correlation of the motion surrogate with the beam delivery sequence enables identification of the motion state in which each of the treatment plan's raster points was irradiated. The original treatment plan is split into quasi-static sub-treatment plans, according to Bert & Rietzel.<sup>27</sup> Each plan comprises all raster points fully or partly irradiated in the respective 4DCT phase. Sorting of the points into associated sub-treatment plans is performed using either the amplitude, the phase or the relative amplitude motion state identification, as discussed above. Let it be emphasized again, that the motion state identification method ideally should match the one used for 4DCT reconstruction.

The generation of sub-treatment plans has been fully re-implemented to integrate the functionality developed by Bert & Rietzel<sup>27</sup> and RDBT according to Lüchtenborg *et al.*<sup>28</sup> in a more robust and general way than the original implementation. As a first step of this procedure, the temporal sequence of BDE is complemented by identification of the valid motion state for each event. Additional events which mark a change of the 4DCT phase, so-called MSC events, are then generated and inserted into the BDS at the respective times.

Generation of the sub-treatment plans is performed by sequential processing of the linked list of BDE. In contrast to earlier implementations, the algorithm employs a state machine approach to more effectively handle transitions between BDE and reliably intercept invalid event transitions being inconsistent with Table 1, e.g., resulting from defective data. The irradiation of each raster point is traced over time and the nominal fluence is sub-divided and allocated to the respective sub-treatment plans. If simulation of beam tracking has been requested, the raster point coordinates are adapted according to the provided tracking look-up table<sup>27</sup>. In the case of RDBT particle fluences are adapted according to Lüchtenborg *et al.*<sup>28</sup> In order to maintain consistency between the simulation and the actual beam delivery, the same routines are also used in the treatment control system. Beam tracking and RDBT both rely on motion monitoring for real-time calculations. Miscorrelation of the true tumor motion and the monitored

motion, such as phase shifts, can be simulated using a dedicated motion monitoring trajectory for all real-time tasks (section II.A.1.).

295 The subsequent distribution of the nominal particle fluences to the motion states is independent from the motion mitigation modality and also applies to uncompensated irradiation. The beam intensity is assumed to be constant over the time-scale of a raster point irradiation (several milliseconds). This is a valid approximation for treatment conditions at HIT and GSI but might require additional refinement in case of more rapid treatment delivery as planned at NIRS or PSI.<sup>15;55</sup> The nominal particle fluence then  
300 is sub-divided according to the relative weight of the irradiation time span in the respective motion state, taking potential beam pauses into account. The procedure is repeated until all raster points of the 3D treatment plan have been processed. Note that solely for beam tracking and RDBT specific steps need to be taken (e.g., beam adaption according to applied tracking parameters). In all other cases the treatment modality characteristics of the beam delivery are communicated by the BDS only (e.g., beam pausing in  
305 case of gating or multiple and quick irradiations in case of rescanning).

The quasi-static sub-treatment plans discussed in the last section are the starting point for 4D dose calculation. The dose calculation algorithm of Gemmel *et al.* was implemented in *TRiP4D* and is capable of both, biological and physical dose calculation. For details the reader is referred to the respective publication.<sup>30</sup> In brief, the dose contributions of all raster points of the respective sub-  
310 treatment plan to each dose voxel are collected in every motion state. For this purpose, the voxel position is transformed accordingly, using *TRiP4D*'s deformation map module and taking into account the radiological density distribution of the respective 4DCT phase. The algorithm therefore is fully compatible with transformation maps obtained from deformable image registration of patient 4DCT. The total physical dose is computed by summation of dose contributions from all motion states in the  
315 reference state. For biological dose calculation the particle spectra in energy and atomic number are also accumulated over all motion states in consideration of the transforming dose grid. The total spectra finally are used as input to the calculation of the relative biological effectiveness and the resulting biologically effective dose using the local effect model (LEM).<sup>22</sup> Accordingly, *TRiP98*'s capabilities to calculate non-linear dose response of radiographic films as a function of local particle and energy  
320 spectra using a model<sup>56</sup> similar to the LEM have been extended to 4D. Additionally, calculation and output of dose and detector response distributions for individual motion states is supported. Finally, *TRiP4D* provides calculation of dose volume histograms (DVH) for VOI in all motion states in conjunction with the 4D segmentation module.

## IV. Verification

325 *TRiP4D* is a newly designed 4DTP extension to the established GSI treatment planning system *TRiP98*. The integration of the 4D functionality required substantial changes of the existing program structure and source code. Systematic testing is required to assure that core functionality of *TRiP98* is not impaired. Moreover, the 4D planning functionality combines newly implemented features and re-  
330 implementations based on earlier programs. Both demand elaborate validation, especially considering the program's possible future application in clinical routine. The consistency of *TRiP98*'s core functionality in *TRiP4D* has been verified successfully using the comprehensive test suit delivered with the mother program and will not be discussed here. The predecessors of *TRiP4D* were repeatedly tested in various dedicated experiments.<sup>24;29;30</sup> Within the scope of this work selected tests were re-iterated and *TRiP4D*'s performance was benchmarked against the experimental results and the predecessor programs.  
335 Additionally, new water phantom experiments were designed and conducted, in order to test the program's combined functionality at a high level of complexity.

### IV. A. Radiographic film response simulations

The 4D treatment simulation capabilities of *TRiP4D* were tested in dose response simulations for radiographic films moved during irradiation. The simulations were verified against experimental results  
340 obtained by Bert *et al.* and were compared to previous simulations of 4D detector response for these experiments.<sup>29</sup>

#### IV. A. 1. Materials and methods

**Experimental setup and conduct:** The experimental setup of the radiographic film measurements is summarized here in brief. For a detailed description the reader is referred to Bert *et al.*<sup>29</sup> Irradiation was performed at GSI with a carbon ion beam and a single-slice treatment plan. The plan was designed to cover a  $110 \times 110 \text{ mm}^2$  field with a homogeneous dose. Radiographic films were used as detectors and mounted on a motorized sliding table in free air. The films were moved sinusoidally during irradiation in left-right direction in beam's-eye-view (BEV). Various motion amplitudes, periods and initial phases were chosen and adjusted via the sliding table. The radiographic films were developed and digitized according to Spielberg *et al.*<sup>56</sup> The film trajectories were measured with sub-millimeter precision and recorded during irradiation with a calibrated camera system tracking an infrared LED at an acquisition rate of 40 Hz. The BDS, i.e. the irradiation times of all raster points and the start (BON) and stop (BOF) times of the beam extraction, were measured in a separate data acquisition system via TTL pulses provided from the control system. In order to establish temporal correlation between the target motion and the BDS, beam status signals were additionally recorded with the motion monitoring system.

**4D film response calculations:** The simulations of the optical film density were carried out using the 4D extensions to the *TRiP98* program by Bert & Rietzel (*TRiPBR*) on the one hand and those of *TRiP4D* on the other. According to section II. C. 3 the simulations were divided into two steps: (i) generation of sub-treatment plans and (ii) calculation of the 4D detector response based on the sub-treatment plans. The two simulation steps were performed with both versions of *TRiP* and in all possible combinations to assess the origin of possibly differing performance. Simulations were performed for 20 motion states and amplitude-based motion state identification. Calculation of the expected optical density of the films in response to the locally deposited dose for both programs is based on the model of Spielberg *et al.* and the resulting particle-specific film responses.<sup>56</sup>

**Data analysis:** The agreement of the simulations with the respective measurement for each set of motion parameters was assessed by statistical analysis of the differential optical density distributions. Rigid registration of the coordinate systems of the measured films and the simulations was used as determined by Bert *et al.*<sup>29</sup> The analysis was restricted to a ROI of a  $155 \times 135 \text{ mm}^2$  and pixels with optical densities  $S > 0.01$ . These criteria establish an individually adjusted analysis mask for each case to prevent domination of the background outside the irradiated area. The relative mean deviation in optical density and its standard deviation were computed and chosen as a figure of merit to evaluate the agreement.

#### IV. A. 2. Results

Table 2 lists the results of the statistical analysis for the 14 measured parameter combinations. Peak-to-peak motion amplitudes range from 8-20 mm for motion periods between 3 and 7 s. The initial phases were 0, 90, 180, 270 degree, depending on the case. In table 2, the analyzed simulation combinations are denoted by the identifiers for the programs used in each of the two simulation steps, *TRiPBR* (BR) and *TRiP4D* (4D), respectively. The comparison of the results for the unmixed configurations "only *TRiPBR*" and "only *TRiP4D*" reveals that the mean relative deviation of simulated and measured optical densities,  $\mu$ , is closer to zero for all 14 cases in the full *TRiP4D* simulations. The largest differences are obtained for cases (a)-(d) with a 20 mm peak-to-peak amplitude ( $>2\%$ ). For case (d) the absolute decrease in  $\mu$  exceeds 7 % and amounts to on average 2 % for all cases. Similarly, the standard deviation  $\sigma$  is reduced for all cases except case (j). The largest decrease in  $\sigma$  is observed for the 20 mm amplitude cases (a)-(d). For case (d) the absolute decrease is larger than 50 % and larger than 7 % for cases (a)-(c). An absolute decrease of around 6 % is yielded for cases (l)-(n), only minor decreases are observed for cases (e)-(i) and (k) ( $<1\%$ ) and a negligible increase for case (j) ( $<0.1\%$ ). The average decrease in  $\sigma$  over all cases amounts to about 7 %.

Results for the mean value and standard deviation in optical density for the mixed simulation *4D/BR* are comparable to those obtained for simulation with *only TRiP4D* in most cases and absolute differences for mean and standard deviation values between *4D/BR* and *only TRiP4D* are below 1 %. Only for case (l) differences of about 1 % and 5 % are observed for the mean and standard deviation, respectively.

Comparing simulations *BR/4D* and *only BR*, both using *TRiPBR* for the generation of sub-treatment plans, the changes in the mean and standard deviation with respect to *only TRiPBR* are much less

395 pronounced than for simulations *4D/BR* and *only TRiP4D*. Only cases (d) and (l) show significant improvements in the mean value ( $>0.8\%$ ) and the standard deviation ( $>5\%$ ).

#### IV. A. 3. Discussion

400 The data in table 2 show that the major improvement in simulation accuracy is due to the new algorithm for the generation of sub-treatment plans in *TRiP4D*. These improvements could be traced back to the more consistent handling of BDS in *TRiP4D* compared to *TRiPBR*. The state machine approach discussed in section II. C. 3 proves less error-prone, in particular in the case of corrupted BDS data. For cases (a)-(d) the defective data resulted from timing issues of the data acquisition at the time of the experiments and could be resolved retrospectively. Using *TRiP4D* instead of *TRiPBR* for 4D dose calculation had a small impact on the agreement of the simulated and measured optical density distributions. The small improvements gained over *TRiPBR* for mean value and standard deviation 405 predominantly result from the avoidance of additional interpolation in *TRiP4D*'s 4D dose calculation, which does not require summation of individually transformed state dose cubes in the reference state. The larger deviations obtained for cases (d) and (l) result from high sensitivity of these cases with respect to minor differences in the applied displacements vectors. Specifically, small film displacements ( $<2\text{ mm}$ ) orthogonal to the motion direction, i.e. up-down BEV, have been neglected for *TRiP4D* 410 calculations as they are affected by large relative errors of the position measurement. On average, the measured optical density distributions are reproduced by the full *TRiP4D* simulations to about  $(-2 \pm 12)\%$ . Hence, the calculated optical densities in general are slightly overestimated by *TRiP4D*. Regarding the accuracy of around  $10\%$  to be expected from film response calculations for ion beams,<sup>56</sup> the simulations otherwise are in good agreement with the measurements.

#### 415 IV. B. Water phantom experiments and simulations

Predecessor versions of the GSI 4DTPS have been tested repeatedly in experiments. So far, 2D target motion with and without range changes introduced by absorbers were studied.<sup>24;29</sup> In preparation of extensive patient treatment planning studies and future clinical application, more elaborate tests of *TRiP4D* were carried out in water phantom experiments at HIT using a robotic setup with 3D target 420 motion and gated beam delivery. *TRiP4D* simulations were compared to absolute 4D dose measurements.

##### IV. B. 1. Materials and methods

**Experimental setup and conduct:** A sketch of the experimental setup is shown in Figure 3. An ellipsoidal target volume of  $82\text{ mm}^3$  was irradiated in a static water phantom with gated beam delivery. 425 The absorbed dose was measured with an array of 24 pinpoint ionization chambers, as reported by Karger *et al.*<sup>57</sup> Three-dimensional sinusoidal motion of the ionization chamber array was facilitated using a robotic arm.<sup>58</sup> Peak-to-peak motion amplitudes of 20 mm in LR BEV and 10 mm in the remaining dimensions were chosen. Additionally, non-gated static reference irradiations were performed. Beam control and the adjustment of the gating window were established using the AZ-773V 430 system of ANZAI Medical Co. Ltd. The gating window was configured based on the signal of a laser distance sensor monitoring the LR projection of the ionization chamber array motion. Gating windows were adjusted to result in residual motion amplitudes of 2-10 mm around the maximum amplitude in LR BEV. The target motion, raster point irradiation times and the beam status signal were acquired with a dedicated data acquisition system.

435 Treatment plans were optimized with the GSI reference 3D treatment planning system *TRiP98*. 18 different combinations of lateral grid spacing (2 and 3 mm), spacing of iso-energy slices (1, 2, 3, and 4 mm), beam full-width at half maximum (6, 8, and 10 mm) and two different ripple-filters (RiFi)<sup>59</sup> were chosen. Apart from the standard RiFi with 3 mm effective Bragg-peak width (RiFi3), two orthogonally 440 crossed 3 mm RiFi were used, approximately corresponding to a 4 mm RiFi (RiFi4). The plans were optimized for a homogeneous target dose of 2 Gy.

Simulations were performed based on the nominal 3D target trajectory as the motion surrogate, the reference treatment plan and the respective BDS according to section II. C. 3. The BDS was obtained by combined evaluation of the measured signals from the treatment and accelerator control systems over time. Generation of the sub-treatment plans was based on the nominal target motion trajectory generated 445 by *TRiP4D*. The individual initial phases  $\phi$  for each measurement caused by the gated beam delivery

were taken into account. 4D physical dose calculations were performed for 22 phases of a computer-generated 4DCT and phase-based motion state identification. The transformation maps for rigid target motion were generated with *TRiP4D* based on the target motion trajectory.

**Data analysis:** The agreement of the simulations with the respective measurements was assessed by statistical analysis of measured and calculated dose values at the ionization chamber positions. For the analysis of the individual measurements the mean relative difference  $\overline{\Delta D}$  of measured  $D^{\text{meas}}$  and calculated  $D^{\text{calc}}$  dose values and its standard deviation,  $\sigma^D$  has been calculated for  $N=22$  of the 24 ionization chamber positions per measurement. The remaining two ionization chambers were neglected for analysis, as they were located close to the target volume boundary (Figure 2). Additionally, a bivariate linear regression model was fitted to the ensemble of measured and simulated dose values for the individual ICs using JMP (version 9.0, SAS Institute Inc., Cary, NC, USA):

$$D^{\text{meas}} \approx \alpha D^{\text{calc}} + \beta R_{3/4} \quad (\text{Equation 1})$$

$R_{3/4}$  denote the constant contributions of the RiFi3 and RiFi4, respectively.  $\alpha$  and  $\beta$  are free parameters. The results of the bivariate regression are reported as the coefficient of variation,  $R^2$ , and the root-mean-square error (RMSE) of the model.

#### IV. B. 2. Results

For each plan three to four irradiations with different motion amplitudes, distributed in the range of 2-10 mm, and one static measurement were performed, resulting in a total of 82 measurements, 64 of them with gated beam delivery. 4D simulations were performed for 52 of the gated irradiations. The remaining 12 cases were removed from the analysis because of gross measurement errors, predominantly missing or deficient BDS data. Figure 2 shows a section through the simulated dose distributions for the static and a representative gated irradiation using the same treatment plan. A gating window of 50 % was used in this case, corresponding to 10 mm peak-to-peak residual motion for the major (LR) motion component. The positions of the ionization chambers used for dose extraction and comparison with the measured data are also indicated in the figure. As expected, the dose distribution for the gated irradiation exhibits significant dose inhomogeneities due to interplay effects. Figure 3 reports the mean relative dose difference and standard deviation between simulated and measured dose values at the 22 ionization chamber positions for all 52 gated measurements, drawn versus the measurement number. The graph is split for 3 and 4 mm effective Bragg-peak width, i.e. RiFi3 and RiFi4, respectively. Two separate fits for the average agreement of all respective measurements are given. The simulations for RiFi3 and RiFi4 on average agree with the measurements within about  $(-1 \pm 4) \%$  and  $(-3 \pm 4) \%$ , respectively. For both RiFi configurations all cases had standard deviations smaller than 8 %, for about 80 % of the cases values smaller than 5 % were found. Simulations of the static reference irradiations on average reproduce the measurement within  $(-2 \pm 2) \%$  for the RiFi3 and  $(-3 \pm 1) \%$  for the RiFi4 treatment plans. Figure 4 summarizes the results of the linear regression according to the model in equation 1. By construction, depending on the RiFi, two different linear fits are obtained. Measured and simulated dose values exhibit an explained variance of  $R^2=0.81$  with an RMSE of the model of 3.4 % ( $p < 10^{-4}$ ). The systematic difference in the intercept for the two RiFi was statistically significant on the  $p < 10^{-4}$  level.

#### IV. B. 3. Discussion

In summary, good overall agreement of the measurements and the 4D simulations was found for both, the analysis for the group of 22 ionization chambers per case and the linear regression for the individual ionization chambers over all cases. The RiFi4 data show a slight systematic deviation in the mean relative dose difference relative to the RiFi3 data of about 1.5 %. This is consistent among gated and stationary experiments and was also reproduced in the fits of the linear regression model. The additional systematics found for the RiFi4 data can most likely be attributed to larger uncertainties in the depth-dose base data<sup>21</sup> in these cases. Furthermore, very small mean deviations of the static from the moving cases of below 1 % were observed (Figure 3), possibly originating from small setup have less impact on the stationary results, due to the smaller gradients. The residual deviations of about 1-2 % observed for the RiFi3 cases are well within the expected systematic uncertainties of 3-3.4 % in absolute ionization chamber dosimetry for heavy ion radiation.<sup>60</sup> With standard deviations of less than 5 % for most cases

the simulations agree well with the measured dose distributions. The increase of about 2 % in standard deviation for the moving relative to the static cases can be attributed to the much higher complexity of the simulations which are subject to numerous influencing factors. For instance, for the employed setup, additional uncertainties can be expected from the measured beam status signals, since, for technical reasons, these were not coupled to the beam monitoring system and feature minor unknown and systematic temporal shifts. Also, signal fluctuations were an issue during data taking. Although most measurements exhibiting the problem were disregarded, residual degradation of the beam delivery sequence data must be expected and should, for instance, have an impact on the calibration of the initial motion phase.

#### IV. C. Biological dose calculation

Biological 4D dose calculation is indispensable in clinical 4DTP for heavy ion therapy. Cell survival experiments have been conducted by Gemmel *et al.* using a dedicated phantom to validate the 4D dose calculation algorithm implemented in a predecessor version of the 4DTPS.<sup>30</sup> This algorithm has been integrated into *TRiP4D* and calculations of the RBE-weighted dose have been re-iterated for one particular experiment (experiment 1 in the original publication). The results are compared to the measurement itself and the results of simulations by Gemmel *et al.*

##### IV. C. 1. Materials and methods

The experimental setup, data acquisition and cell processing are introduced here in brief. The reader is referred to the original publication for a detailed description.<sup>30</sup> A biological phantom with Chinese hamster ovary cells (CHO-K1) in a medium was positioned on a sliding table and irradiated with a carbon ion beam. The treatment plan was optimized for a homogeneous dose of 6 Gy(RBE) in a cuboid volume of  $28 \times 23 \times 45 \text{ mm}^3$ . During irradiation the table was moved sinusoidally with a 40 mm peak-to-peak amplitude in left-right BEV to induce interplay effects. Changes of the radiological depth were introduced by a stationary ramp-shaped absorber in front of the phantom. Motion monitoring, acquisition of the BDS and time correlation of the table motion and the irradiation progress were performed as for the radiographic film experiments discussed in the previous section. After irradiation, 10 cell samples were chosen for further analysis. Absolute cell survival was determined according to Puck and Markus<sup>61</sup> and was converted to RBE-effective dose.

Calculation of RBE-effective dose and cell survival were performed based on the recorded BDS and the motion monitoring data using both, the program of Gemmel *et al.* (*TRiPG*) and *TRiP4D*. As for the simulations of radiographic film response in the previous section simulations were performed in two steps: (i) generation of sub-treatment plans and (ii) calculation of the 4D biological dose on the basis of the sub-treatment plans. Since *TRiPG* relies on the TPS of Bert & Rietzel<sup>27</sup> (*TRiPBR*) for the generation of sub-treatment plans, step (i) was performed with the latter and *TRiP4D*, respectively. Resulting sub-treatment plans then were used as input to either *TRiPG*'s and *TRiP4D*'s dose calculation in step (ii). The same computer-generated 4DCT with 11 motion states as used by Gemmel *et al.* was employed for all calculations. Biological dose calculation was carried out according to section II. C. 3 and Gemmel *et al.*<sup>30</sup> The physical dose was computed with either a standard pencil beam algorithm and an advanced algorithm including multiple scattering effects.<sup>62</sup> The rigid deformation maps for *TRiP4D* and *TRiPG* were created based on the acquired motion monitoring data. Additional 4D pseudo-static simulations were performed with both programs using identity deformation maps. These serve to decouple the deformation of the dose grid and the accumulation of the particle spectra over all motion states from each other in the calculations. In this way, 3D dose calculation is mimicked. The resulting pseudo-static dose distributions were compared to the static dose distribution obtained for the treatment plan with the *TRiP98* reference TPS. The same set of depth-dose and particle spectra data<sup>21</sup>, as well as the same version of the Local Effect Model<sup>63</sup> was used in all 3D and 4D simulations to guarantee comparability. The measured RBE-effective dose values from Gemmel *et al.* were compared to the corresponding simulations for the cell samples. The difference in RBE-effective dose was calculated for each sample  $i$ :  $\Delta D_i = D_i^{\text{meas}} - D_i^{\text{calc}}$ . The mean difference  $\overline{\Delta D}$  and its standard deviation  $\overline{\sigma}^D$  were determined to assess the agreement of the different simulations with the measurement.

##### IV. C. 2. Results

Table 2 lists the results of the statistical analysis of the differences in measured and simulated RBE-effective dose. The simulation results for the pencil beam dose algorithm (PB) are consistent for all three

550 simulations and are independent of the program used for generation of the sub-treatment plans. For the multiple scattering algorithm (MS) and simulation BR/G the results published by Gemmel *et al.* were reproduced. Simulations BR/4D and “only *TRiP4D*” both using *TRiP4D*'s dose calculation, however, show a significant systematic discrepancy of about 310 mGy (RBE) for the mean difference in RBE-effective dose with respect to simulation BR/G. Table 3 summarizes the observed maximum dose differences between the 4D pseudo-static and the static reference dose distribution of *TRiP98*. For the MS algorithm the comparison of the pseudo-4D dose distribution attained with configuration BR/G and the static dose distribution reveal maximum absolute dose differences per voxel,  $|\Delta D_{\max}|$ , of more than 750 mGy (RBE). In contrast, for simulation BR/4D differences of less than  $10^{-2}$  mGy (RBE) were found. For algorithm PB the respective dose distributions agree within less than  $10^{-2}$  mGy (RBE) for both, 555 simulations BR/G and BR/4D. Also, compared to the dose distributions obtained with *TRiP4D*, less lateral dose contributions outside the target volume were observed by visual inspection. Finally, the comparison of the static reference dose distributions for algorithms PB and MS on average showed about 70 mGy (RBE) ( $\approx 1\%$ ) less dose in the target region due in case of MS, due to lateral scattering. The differences in dose found between the two algorithms in the BR/4D simulations of around 560 60 mGy (RBE) are in agreement with this fact (c.f. Table 2). For the target dose of 6 Gy (RBE) the mean deviation of  $(617 \pm 538)$  mGy (RBE) for the *TRiP4D* simulation w.r.t. the measurement translates into a relative deviation of  $(10 \pm 9)\%$ . The average error in RBE-effective dose propagated from the cell survival measurement error was estimated to about 24%. Thus, the simulation results are well compatible with the measurement.

#### 570 IV. C. 3. Discussion

Even though the simulations show better agreement with the measurement for configuration BR/G, the performed tests indicate that *TRiPG*'s dose calculation algorithm is inaccurate when using the multiple scattering physical dose calculation algorithm. 4D pseudo-static dose calculations provide the possibility to assess the performance of 4D dose calculation independently of the dose grid transformation and 575 allow for comparison with the static reference dose distributions. In these simulations static dose distributions were reproduced by *TRiP4D* to a high level of precision for both the PB and MS algorithm. Since the implementation of biological dose calculation is decoupled from the implementation of the PB and MS physical dose calculation algorithms and is used downstream of these calculations, the issues observed for the MS algorithm most likely do not originate from specific calculations to determine the BED. This is supported by the fact that for the PB dose algorithm results are comparable to those 580 obtained with *TRiPG*. In contrast to the radiographic film experiments, no significant improvement was obtained using *TRiP4D* for the generation of sub-treatment plans (configuration “only *TRiP4D*”). Since the BDS in this case was not affected by any data acquisition issues, *TRiP4D*'s more robust algorithms did not yield any advantage over *TRiPBR* with respect to simulation accuracy.

### 585 V. Discussion

In the previous sections the development and implementation of *TRiP4D*, a 4D treatment planning system for scanned ion beams have been discussed. The program is based on the GSI in-house treatment planning system *TRiP98* which has been used successfully for clinical treatment planning during the GSI pilot project.<sup>21;23</sup> The main objective of this work was the integration of previous 4DTP efforts and 590 developments made at GSI and the further advancement of the program towards a clinically serviceable 4DTPS. Previous treatment planning developments of Bert & Rietzel and Gemmel *et al.* in parts have served as prototypes.<sup>27;30</sup> The new TPS enables realistic clinical treatment planning with multiple fields and is compatible with the treatment planning workflow used at the Heidelberg Ion Beam Therapy Center.

595 4D treatment planning in *TRiP4D* is based on 4DCT, deformable image registration and 4D segmentation to model the moving patient anatomy. These tools have become well established over the past years not only in 4DTP for photon therapy<sup>4;26</sup> but also for particle therapy<sup>7;8;16;64</sup>. Hence, emphasis was put on a flexible integration of these instruments to explicitly allow for realistic patient treatment planning. Interfaces to several image registration software packages have been implemented and permit 600 quantitative assessment of 4DCT data based on the resulting deformation maps. The corresponding structures were developed with a focus on principal compatibility with a wide range of registration

algorithms and programs. The use of additional registration software packages in the future, thus, is expected to be manageable with a minimum effort. Furthermore, 4D segmentation functionality has been newly implemented. A novel 4D contour data model has been introduced which employs the representation of contours as VBM, i.e. the VOIs are stored in a bit-wise fashion using a CT-like data format. This enables to store 4D segmentation data as a single entity and avoids use of multiple incoherent sets of polygonal contours. Additionally, a 4D contour propagation algorithm based on deformable image registration has been implemented being capable of creating a full 4D segmentation dataset starting from a manually contoured reference phase. Many other groups have made efforts on the implementation of 4D contour propagation algorithms. Commonly, the approaches are divided into registration-driven<sup>26;38</sup> and deformable model-driven<sup>45;46</sup> techniques. In the first approach the deformation field gives guidance to contour deformation, while in the second approach a physical model is used to iteratively match the contours to the image features. *TRiP4D* relies on the former approach, since available deformation maps can be efficiently re-used. The implemented contour propagation algorithm employs the inverse deformation maps and the reference phase contour to determine the VOI in each 4DCT phase as a VBM. An alternative strategy has, for instance, been published by Lu *et al.*<sup>38</sup> They have used triangular meshes to model the surface of the VOI. After surface deformation the polygon-based contours for all 4DCT phases are generated by performing sections of the surface model with the image plane of interest. A drawback of *TRiP4D*'s propagation algorithm is the necessity to generate both the original (needed for 4D dose calculation) and the inverse deformation maps, as *TRiP4D* does not support inversion of deformation maps. Since the registration process can be sufficiently automated, this does not appear as a major limiting factor. It can be anticipated that the use of VBMs is more memory consumptive compared to, e.g., triangular meshes. Whilst the VBM contour model has the advantage that contours can be easily combined and manipulated, e.g., for ITV generation, the resolution of the contours is forced to the regular CT grid, causing a loss of precision. However, since the usual lateral CT voxel spacing and the expected registration accuracy are on the order of millimeters,<sup>65</sup> no significant impact is expected. Nevertheless, also up-sampled VBM datasets can be used in *TRiP4D* at the expense of memory consumption.

With respect to 4D optimization of treatment plans, *TRiP4D* incorporates previous work of our group with respect to beam tracking<sup>27;28</sup> and for the generation of ITVs that incorporate the range domain and still allow intensity modulated optimization.<sup>50</sup> The new developments further set the stage for more elaborate techniques similar to 4D dose optimization concepts that have been investigated, e.g., by Nohadani *et al.*<sup>66</sup> or Unkelbach *et al.* who incorporated robustness considerations.<sup>67</sup>

4D treatment simulation functionality was implemented similarly to the previous 4D versions of *TRiP* but with improved algorithms using generalized beam delivery events (BDE) and state machines that check the consistency of the beam delivery sequence (BDS). Re-assessment of existing experimental data used to verify previous versions of *TRiP* showed the BDE based distribution of beam positions into motion states results into improved agreement to experimental data. Furthermore, the biological 4D dose calculation algorithm of Gemmel *et al.*<sup>30</sup> has been updated to the most advanced version of the multiple scatter dose calculation algorithm.<sup>62</sup> Re-analysis of existing verification data showed flaws in the initial implementation but did not change the conclusions of the previous study. The algorithm is similar to the one of Boye *et al.*<sup>14</sup> and Paganetti *et al.*<sup>19</sup> for proton dose calculation, i.e. it uses the deformation field to deform the dose grid rather than the raster grid as originally implemented by Bert & Rietzel for 4D calculation of the absorbed dose, only. The algorithm does not spatially interpolate dose accumulation as proposed by Kraus *et al.*<sup>17</sup>

*TRiP4D*'s 4D simulation functionality has been extensively tested in verification experiments. The preceding sections have presented results of the verification of the full 4D treatment simulation chain, including 4D dose and detector response. As mentioned above, handling of BDS is more robust in *TRiP4D* and implementation of the most recent multiple scattering version changed the results of Gemmel *et al.* at reasonable agreement with the measured RBE-effective dose values. Moreover, new elaborate water phantom experiments were conducted to test *TRiP4D*'s simulation capabilities for 3D target motion, gated beam delivery and a large number of plan parameters and motion configurations. The comparison of measured and simulated dose values showed good agreement standard deviations smaller than 5 % in most cases. It can be concluded that 4D simulations subsequent to treatment delivery are well feasible in experimental setups, provided all necessary parameters are known, i.e. in particular the time structure of the beam delivery process and the target motion during delivery.

However, simulation prior to treatment delivery is very challenging even for simple setups and well known target motion. Synchrotron accelerator systems like those used at GSI and HIT are subject to significant variability of beam availability and the delivered intensity on a sub-second time-scale.<sup>68</sup>

660 These parameters affect the 4D dose deposition substantially, while being difficult to model. Intensity-controlled beam extraction for synchrotrons<sup>69</sup> is a promising development to reduce this kind of uncertainty and currently established at HIT<sup>70</sup>. For patient treatments additional complexity is introduced, since prediction of the target motion in general is not feasible on a time-scale beyond several hundred milliseconds.<sup>71;72</sup> Hence, a reliable prediction of the delivered dose prior to treatment is difficult to achieve. Nevertheless, 4D treatment simulation offers great potential for 4DTP and quality assurance. It may, for instance, provide the opportunity to monitor the success of the plan delivery, if the beam delivery time structure and the patient motion during treatment are measured. Furthermore, in-advance treatment planning simulations can be performed for many different scenarios. Even though the precise configuration of the patient motion and the time structure of the beam delivery is not known, simulations of a wide range of parameter settings, such as different breathing patterns or beam delivery schemes, can be performed and yield a spectrum of possible treatment outcomes. These simulations also can be used to assess plan robustness or define parameters needed as input for the respective treatment delivery technique, such as the number of required rescans or the gating window.

675 It should be emphasized that from a technical point of view there is no principal difference between in-advance simulations in *TRiP4D* and those performed subsequent to treatment. The uncertainty and value of the 4D treatment simulations solely depends on the reliability of the input data. It is important to realize that the accuracy of any 4D treatment planning attempt based on 4DCT and deformable image registration depends decisively on the validity and reproducibility of the input data, in particular between the time of imaging and treatment delivery.<sup>73-75</sup> One important and often neglected aspect of 4D treatment planning was raised by Zhang *et al.* in a very recent publication.<sup>16</sup> They performed 4D scanned proton beam treatment studies for liver tumors investigating the effect of the registration algorithm used for 4D dose calculation. For two established registration tools, mean (maximal) dose differences of 2.9 % (32.8 %) were found for single field irradiations that reduced to 0.57 % (15.2 %) if rescanning is used. 4D dose distributions should thus be assessed being aware that even more parameters influence the calculation than in 3D dose calculations. Hild *et al.* provide visualization tools to quantify and communicate the uncertainty in 4D dose calculation.<sup>76</sup>

## VI. Conclusion

690 We have developed and implemented a novel 4DTP extension to our in-house TPS TRiP98. The software includes state-of-the-art treatment planning methodologies such as 4DCT, 4D deformable registration data, 4D segmentation and contour propagation. We also established compatibility to clinically provided motion monitoring data and beam delivery sequence data allowing for detailed 4D treatment simulations in a clinical environment. The new software further integrates previous 4D treatment planning efforts by our group, comprising multiple-field ITV design including range changes and 4D optimization of beam tracking and dose compensation parameters. The program has been validated in detailed experiments confirming high accuracy of 4D physical and biologically effective dose calculation as well as 4D film response calculations.

## VII. Acknowledgements

700 We thank the German Research Foundation (DFG) for funding this work as part of the Clinical Research Group (KFO) 214. We also appreciate the support of Katia Parodi from HIT who provided the beam base data for the treatment reconstructions.

## VIII. Tables

**Table 1** Types of general beam delivery events (BDE). The chronology of BDE defines the beam delivery sequence (BDS).

event type	characterization	possible transition to
BON	beam on	BOF, NXP
NXP	end of raster point	NXP, EOP, BOF
EOP	end of iso-energy slice	BOF
BOF	beam off	BON

705 **Table 2** Results of the statistical analysis of the agreement between simulated and measured optical film densities for all 14 motion parameter sets (amplitude  $A$ , period  $T$ , initial phase  $\phi$ ). In the four columns the mean relative deviation  $\mu$  of the simulated from the measured densities and its standard deviation  $\sigma$  are reported for all studied program combinations in the two successive simulation steps: generation of sub-treatment plans and 4D detector response calculations. BR and 4D denote the used program for each step, TRiPBR and TRiP4D, respectively.

case	motion parameters			only TRiPBR		Only TRiP4D		BR/4D		4D/BR	
	$A$ [mm]	$T$ [s]	$\phi$ [deg]	$\mu$ [%]	$\sigma$ [%]	$\mu$ [%]	$\sigma$ [%]	$\mu$ [%]	$\sigma$ [%]	$\mu$ [%]	$\sigma$ [%]
(a)	20	5	90	-5.03	20.64	-2.14	12.98	-4.76	20.35	-2.42	13.66
(b)	20	5	0	-7.32	21.52	-3.73	13.23	-7.28	21.66	-3.88	13.35
(c)	20	7	0	-4.80	21.76	-1.46	9.72	-4.76	21.92	-1.59	9.66
(d)	20	7	90	-9.84	68.98	-2.19	12.68	-8.96	56.94	-2.24	12.21
(e)	15	3	0	-1.85	10.78	-0.55	10.48	-1.70	10.71	-0.68	10.54
(f)	15	3	90	-0.89	11.53	0.37	10.84	-0.77	11.50	0.24	10.92
(g)	15	4	0	-3.50	12.06	-2.13	11.68	-3.36	11.96	-2.24	11.68
(h)	15	4	90	-4.39	11.19	-2.89	10.73	-4.21	11.04	-3.06	10.87
(i)	15	5	0	-5.40	14.99	-4.06	14.55	-5.19	14.66	-4.17	14.66
(j)	15	5	180	-5.74	12.74	-4.43	12.78	-5.65	12.86	-4.53	12.65
(k)	15	5	270	-6.46	16.09	-5.11	16.01	-6.38	16.31	-5.21	15.82
(l)	8	5	0	-2.24	18.53	0.12	12.78	-1.04	12.94	-1.02	18.11
(m)	8	4	0	-2.83	15.56	-0.88	9.43	-2.69	15.53	-1.00	9.47
(n)	8	3	0	-2.98	16.92	-1.11	10.93	-2.75	15.71	-1.21	10.89

710 **Table 3** Mean difference  $\overline{\Delta D}$  and standard deviation  $\overline{\sigma}^D$  of measured and calculated RBE-effective doses for the cell samples. BR, 4D, and G denote the programs TRiPBR, TRiP4D and TRiPG used for generation of sub-treatment plans or 4D biological dose calculation, respectively. For each configuration a standard pencil beam (PB) and a multiple scattering (MS) algorithm were tested for physical dose calculation. The highlighted result (\*) was originally published by Gemmel *et al.*<sup>30</sup>. All results are given in mGy (RBE).

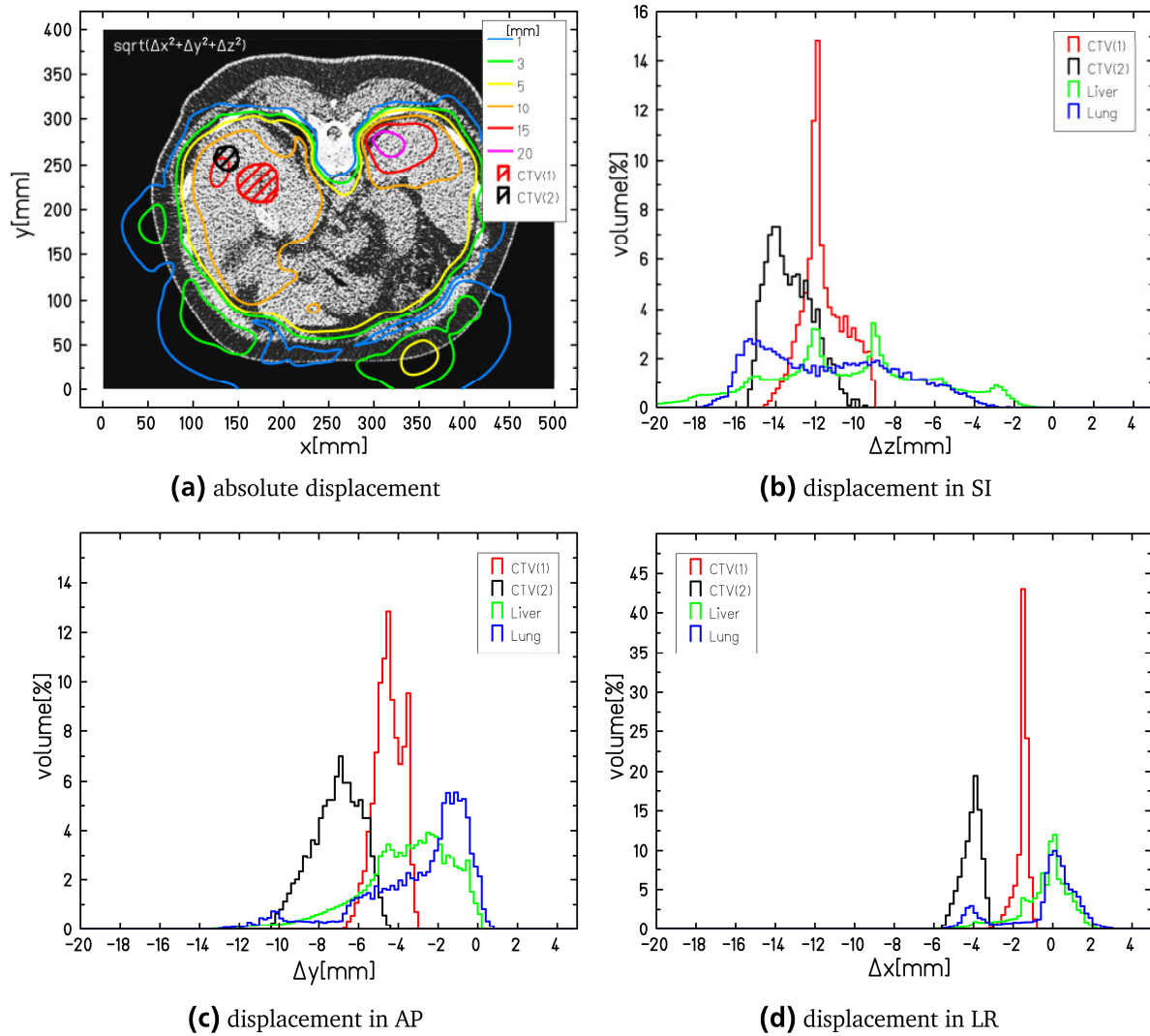
715

simulation	algorithm PB	algorithm MS
	$\overline{\Delta D} \pm \overline{\sigma}^D$	$\overline{\Delta D} \pm \overline{\sigma}^D$
BR/G	-676±642	-298±500*
BR/4D	-676±641	-614±533
only TRiP4D	-679±647	-617±538

**Table 4** Maximum deviations in RBE-effective dose,  $|\Delta D_{\max}|$ , of the 4D pseudo-static dose distributions from the static reference dose distribution for the two dose algorithms, PB and MS. Identity transformation maps were used to mimic 3D dose calculation. The static reference dose distributions were obtained with *TRiP98*. All results are given in mGy (RBE).

simulation	algorithm PB	algorithm MS
	$ \Delta D_{\max} $	$ \Delta D_{\max} $
BR/G	$1.67 \cdot 10^{-3}$	757
BR/4D	$1.67 \cdot 10^{-3}$	$1.43 \cdot 10^{-3}$

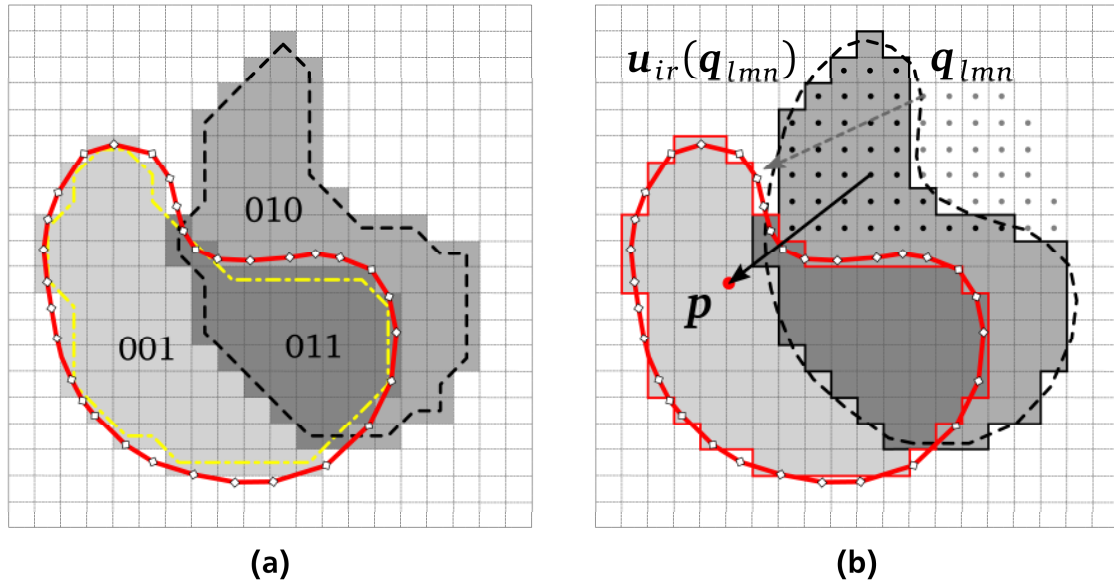
## IX. Figures



725

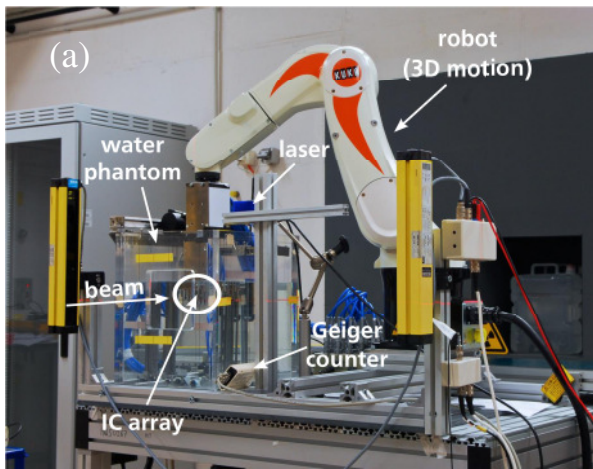
730

**Figure 1** Visualization and assessment of organ motion using deformation maps from deformable image registration in TRiP4D. (a) Axial cut of the reference state CT (end exhale) and the overlaid displacement field between the extreme states, end exhale and end inhale are shown. The absolute values of the displacement vectors are shown as a contour plot, CTV contours of a liver tumor are also indicated. (b)-(d) Histograms of the displacement vector components for the two CTV volumes, liver and lung in the SI, AP and LR direction, respectively. Organ motion is most pronounced in the SI direction and is significantly higher in the CTV(2) than in the CTV(1) volume for all vector components.



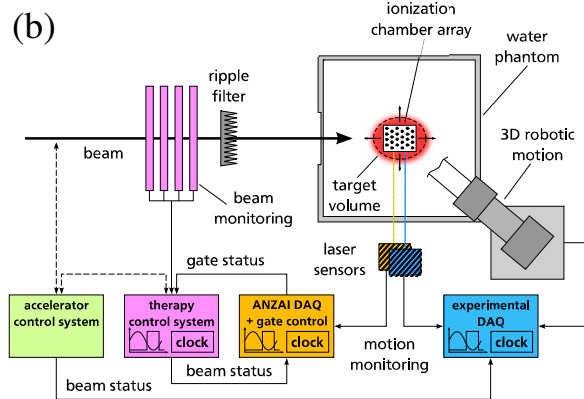
735

**Figure 2** (a) VOI conversion from the polygonal contour (red solid line) into VBM (gray areas) and re-converted polygon contours (dashed lines). The resulting Boolean masks are indicated for the two VOI areas and the overlap region as an example. (b) Contour propagation by inverse transformation from a regular grid. The propagated VOI (dark gray) is formed from voxels with source points inside the polygon contour (red solid line). The arrows indicate example transformation vectors for two voxels.



740

**Figure 3** Sketch of the experimental setup. A robotic arm facilitates 3D motion of a dosimeter array inside the water phantom. Redundant monitoring of the BEV LR motion is performed with two laser distance sensors. The data communication between the gating control unit (ANZAI system), the control system and the experimental data acquisition system is also indicated.



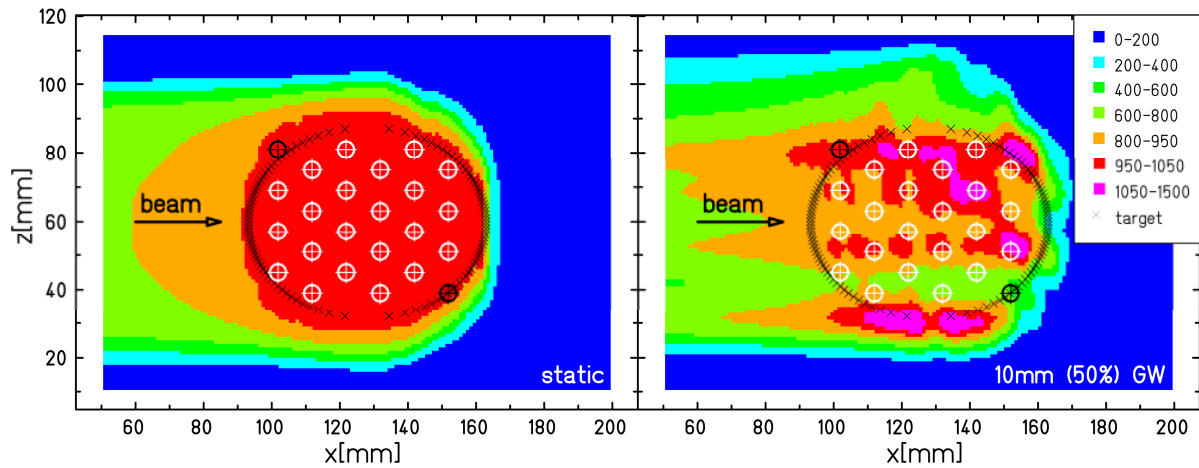


**Figure 4** Bird's eye view section of simulated dose distributions through the center of the target volume for static (left) and gated (right) irradiation with the same treatment plan (lateral grid spacing: 2 mm, IES spacing: 3 mm, beam FWHM: 10 mm, 3 mm RiFi). The 4D dose distribution was transformed to the reference phase (scale in mGy). The positions of the ionization chambers used for dose extraction are indicated by the white and black (neglected for analysis) crosses.

745

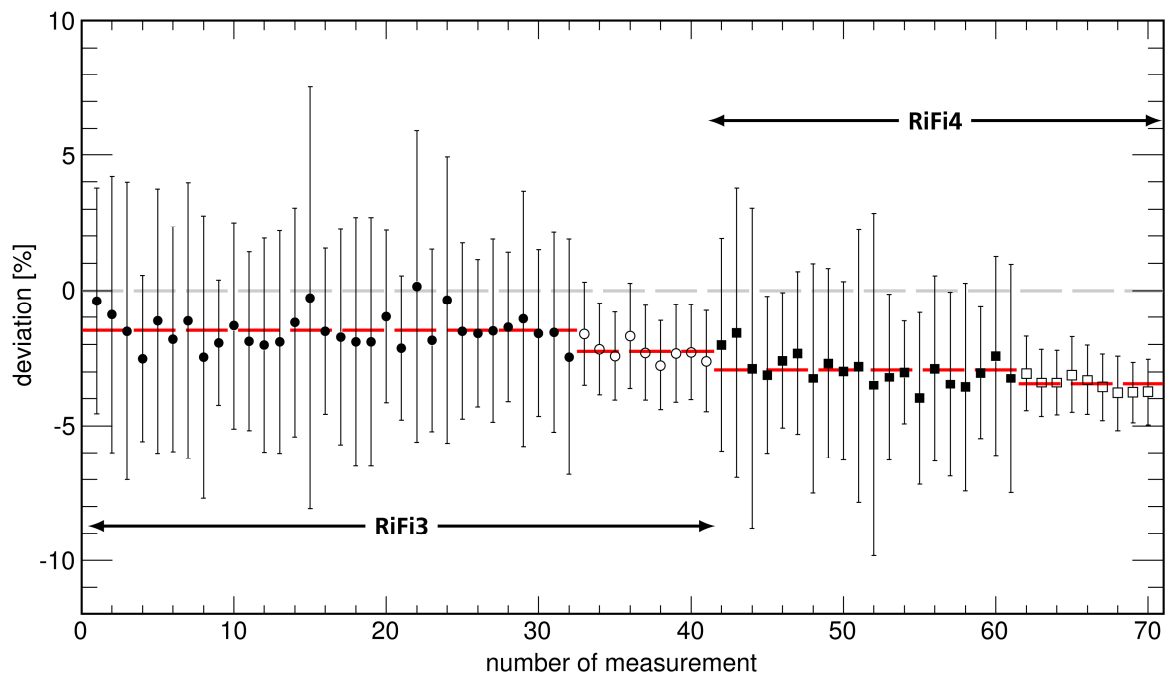


**Figure 5** Agreement of simulated and measured 4D dose distributions for the 52 gated and the 18 static cases (open symbols). Mean and standard deviation of the relative difference between simulated and measured dose values of the 22 ionization chambers are drawn versus the measurement index. The RiFi3 (circles) and RiFi4 (squares) measurements exhibit different systematic deviations from zero, indicated by the fits (red dashed lines).

750

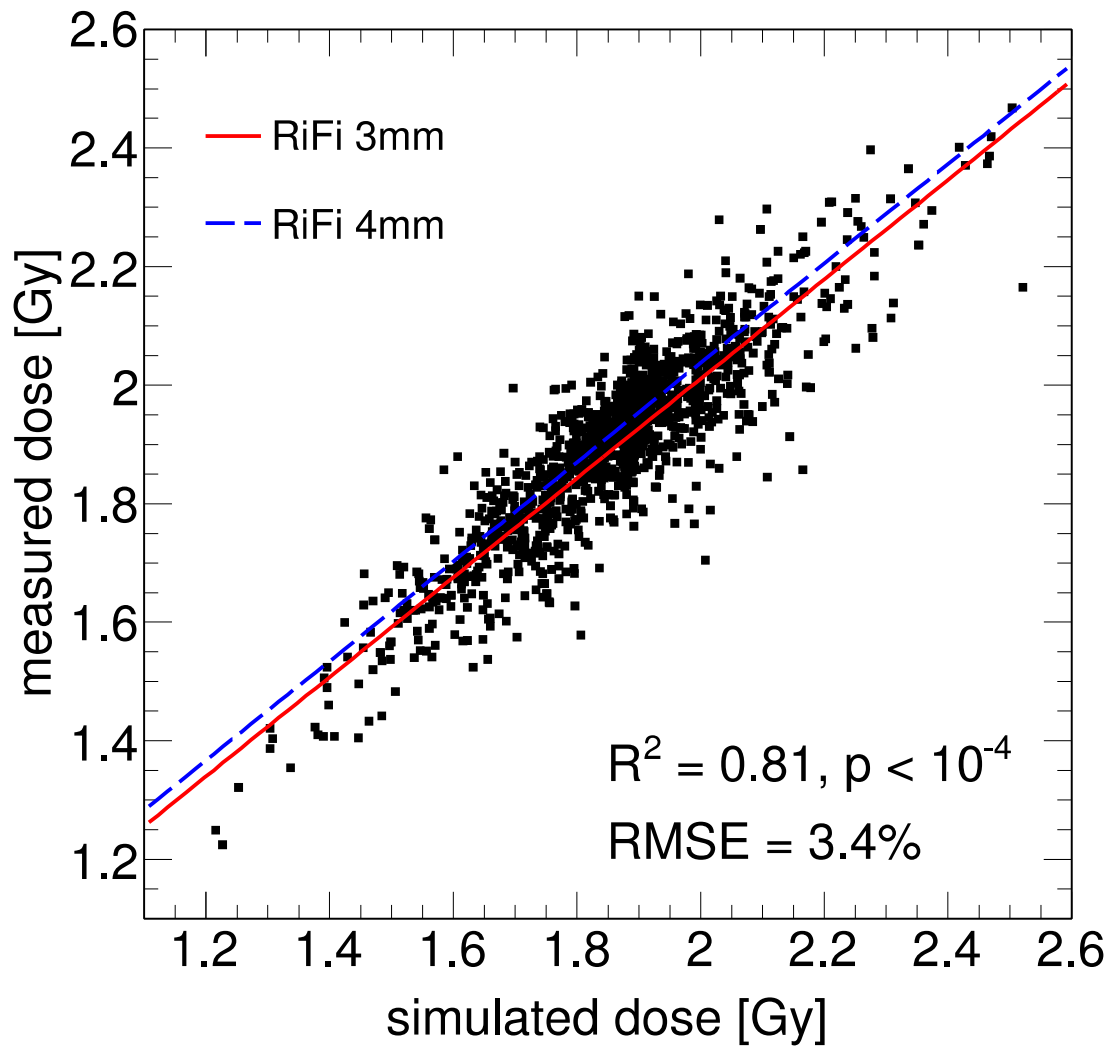


**Figure 6** Scatter plot of the measured ( $D^{\text{meas}}$ ) versus the simulated dose values ( $D^{\text{calc}}$ ) at the individual positions of the ionization chambers for all stationary and gated irradiations. The linear fits determined with the regression model in **Equation 1** are overlaid for RiFi3 (red solid line) and RiFi4 (blue dashed line).

## X. References

- 1 Keall PJ, "4-dimensional computed tomography imaging and treatment planning" *Semin Radiat Oncol* **14**, 81-90 (2004).
- 760 2 Knopf A, Bert C, Heath E, Nill S, Kraus K, Richter D, et al., "Special report: Workshop on 4D-treatment planning in actively scanned particle therapy---Recommendations, technical challenges, and future research directions" *Med Phys* **37**, 4608-14 (2010).
- 3 Chen GT, Kung JH, Rietzel E, "Four-dimensional imaging and treatment planning of moving targets" *Front Radiat Ther Oncol* **40**, 59-71 (2007).
- 765 4 Keall PJ, Joshi S, Vedam SS, Siebers JV, Kini VR, Mohan R, "Four-dimensional radiotherapy planning for DMLC-based respiratory motion tracking" *Med Phys* **32**, 942-51 (2005).
- 5 Minohara S, Kanai T, Endo M, Noda K, Kanazawa M, "Respiratory gated irradiation system for heavy-ion radiotherapy" *Int J Radiat Oncol* **47**, 1097-103 (2000).
- 6 Koto M, Miyamoto T, Yamamoto N, Nishimura H, Yamada S, Tsujii H, "Local control and recurrence of stage I non-small cell lung cancer after carbon ion radiotherapy" *Radiother Oncol* **71**, 147-56 (2004).
- 770 7 Engelsman M, Rietzel E, Kooy HM, "Four-dimensional proton treatment planning for lung tumors" *Int J Radiat Oncol Biol Phys* **64**, 1589-95 (2006).
- 8 Kang Y, Zhang X, Chang JY, Wang H, Wei X, Liao Z, et al., "4D Proton treatment planning strategy for mobile lung tumors" *Int J Radiat Oncol Biol Phys* **67**, 906-14 (2007).
- 775 9 Mori S, Chen GT, "Quantification and visualization of charged particle range variations" *Int J Radiat Oncol Biol Phys* **72**, 268-77 (2008).
- 10 Mori S, Wolfgang J, Lu HM, Schneider R, Choi NC, Chen GTY, "Quantitative Assessment of Range Fluctuations in Charged Particle Lung Irradiation" *Int J Radiat Oncol* **70**, 253-61 (2008).
- 11 Phillips MH, Pedroni E, Blattmann H, Boehringer T, Coray A, Scheib S, "Effects of respiratory motion on dose uniformity with a charged particle scanning method" *Phys Med Biol* **37**, 223-33 (1992).
- 780 12 Bert C, Grözinger SO, Rietzel E, "Quantification of interplay effects of scanned particle beams and moving targets" *Phys Med Biol* **53**, 2253-65 (2008).
- 13 van de Water S, Kreuger R, Zenklusen S, Hug E, Lomax AJ, "Tumour tracking with scanned proton beams: assessing the accuracy and practicalities" *Phys Med Biol* **54**, 6549-63 (2009).
- 785 14 Boye D, Lomax A, Knopf A. 4D dose calculation for scanned proton beams using a deforming dose grid and simulated 4D CT. *Radiotherapy and oncology : journal of the European Society for Therapeutic Radiology and Oncology* **99**, S151-S152. »
- 15 Knopf AC, Hong TS, Lomax A, "Scanned proton radiotherapy for mobile targets-the effectiveness of re-scanning in the context of different treatment planning approaches and for different motion characteristics" *Phys Med Biol* **56**, 7257-71 (2011).
- 790 16 Zhang Y, Boye D, Tanner C, Lomax AJ, Knopf A, "Respiratory liver motion estimation and its effect on scanned proton beam therapy" *Phys Med Biol* **57**, 1779-95 (2012).
- 17 Kraus KM, Heath E, Oelfke U, "Dosimetric consequences of tumour motion due to respiration for a scanned proton beam" *Phys Med Biol* **56**, 6563-81 (2011).
- 795 18 Paganetti H, Jiang H, Adams JA, Chen GT, Rietzel E, "Monte Carlo simulations with time-dependent geometries to investigate effects of organ motion with high temporal resolution" *Int J Radiat Oncol* **60**, 942-50 (2004).
- 19 Paganetti H, Jiang H, Trofimov A, "4D Monte Carlo simulation of proton beam scanning: modelling of variations in time and space to study the interplay between scanning pattern and time-dependent patient geometry" *Phys Med Biol* **50**, 983-90 (2005).
- 20 Bert C, Durante M, "Motion in radiotherapy: particle therapy" *Phys Med Biol* **56**, R113-R144 (2011).

- 800 21 Krämer M, Jäkel O, Haberer T, Kraft G, Schardt D, Weber U, "Treatment planning for heavy-ion radiotherapy: physical beam model and dose optimization" *Phys Med Biol* **45**, 3299-317 (2000).
- 22 Krämer M, Scholz M, "Treatment planning for heavy-ion radiotherapy: calculation and optimization of biologically effective dose" *Phys Med Biol* **45**, 3319-30 (2000).
- 805 23 Jäkel O, Krämer M, Karger CP, Debus J, "Treatment planning for heavy ion radiotherapy: clinical implementation and application" *Phys Med Biol* **46**, 1101-16 (2001).
- 24 Li Q, Grözinger SO, Haberer T, Rietzel E, Kraft G, "Online compensation of target motion with scanned particle beams: simulation environment" *Phys Med Biol* **49**, 3029-46 (2004).
- 25 Grözinger SO, Rietzel E, Li Q, Bert C, Haberer T, Kraft G, "Simulations to design an online motion compensation system for scanned particle beams" *Phys Med Biol* **51**, 3517-31 (2006).
- 810 26 Rietzel E, Chen GTY, Choi NC, Willet CG, "Four-dimensional image-based treatment planning: Target volume segmentation and dose calculation in the presence of respiratory motion" *Int J Radiat Oncol* **61**, 1535-50 (2005).
- 27 Bert C, Rietzel E, "4D treatment planning for scanned ion beams" *Radiat Oncol* **2**, 24 (2007).
- 28 Luchtenborg R, Saito N, Durante M, Bert C, "Experimental verification of a real-time compensation functionality for dose changes due to target motion in scanned particle therapy" *Med Phys* **38**, 5448 (2011).
- 815 29 Bert C, Richter D, Durante M, Rietzel E, "Scanned carbon beam irradiation of moving films: comparison of measured and calculated response" *Radiat Oncol* **7**, 55 (2012).
- 30 Gemmel A, Rietzel E, Kraft G, Durante M, Bert C, "Calculation and experimental verification of the RBE-weighted dose for scanned ion beams in the presence of target motion" *Phys Med Biol* **56**, 7337-51 (2011).
- 820 31 Schlegel W, Pastyr O, Bortfeld T, Becker G, Schad L, Gademann G, et al., "Computer systems and mechanical tools for stereotactically guided conformation therapy with linear accelerators" *Int J Radiat Oncol Biol Phys* **24**, 781-7 (1992).
- 32 Lujan AE, Larsen EW, Balter JM, Haken RKT, "A method for incorporating organ motion due to breathing into 3D dose calculations" *Med Phys* **26**, 715-20 (1999).
- 33 Rietzel E, Chen GTY, "Deformable registration of 4D computed tomography data" *Med Phys* **33**, 4423-30 (2006).
- 825 34 Kessler ML, "Image registration and data fusion in radiation therapy" *Br J Radiol* **79 Spec No 1:S99-108.**, S99-108 (2006).
- 35 Yang D, Lu W, Low DA, Deasy JO, Hope AJ, El N, I, "4D-CT motion estimation using deformable image registration and 5D respiratory motion modeling" *Med Phys* **35**, 4577-90 (2008).
- 36 Sharp GC, Kandasamy N, Singh H, Folkert M, "GPU-based streaming architectures for fast cone-beam CT image reconstruction and demons deformable registration" *Phys Med Biol* **52**, 5771-83 (2007).
- 830 37 Veblen O, Young JW. *Projective Geometry*. Ann Arbor, Michigan: University of Michigan Library; 2005.
- 38 Lu W, Olivera GH, Chen Q, Chen ML, Ruchala KJ, "Automatic re-contouring in 4D radiotherapy" *Phys Med Biol* **51**, 1077-99 (2006).
- 835 39 Gaede S, Olsthoorn J, Louie AV, Palma D, Yu E, Yaremko B, et al., "An evaluation of an automated 4D-CT contour propagation tool to define an internal gross tumour volume for lung cancer radiotherapy" *Radiother Oncol* **101**, 322-8 (2011).
- 40 Glassner A. *An introduction to ray tracing*. Morgan Kaufmann; 1989.
- 41 Hales TC, "The jordan curve theorem, formally and informally" *The American Mathematical Monthly* **114**, 882-94 (2007).
- 42 Freeman H, Davis LS, "A Corner-Finding algorithm for Chain-Coded curves" *IEEE Transactions on Computers C* **26**, 297-303 (1977).
- 840 43 Ragan D, Starkschall G, McNutt T, Kaus M, Guerrero T, Stevens CW, "Semiautomated four-dimensional computed tomography segmentation using deformable models" *Med Phys* **32**, 2254-61 (2005).

- 44 Shekhar R, Lei P, Castro-Pareja CR, Plishker WL, D'Souza WD, "Automatic segmentation of phase-correlated CT scans through nonrigid image registration using geometrically regularized free-form deformation" *Med Phys* **34**, 3054-66 (2007).
- 845 45 McInerney T, Terzopoulos D, "Deformable models in medical image analysis: a survey" *Med Image Anal* **1**, 91-108 (1996).
- 46 Montagnat J, Delingette H, "4D deformable models with temporal constraints: application to 4D cardiac image segmentation" *Med Image Anal* **9**, 87-100 (2005).
- 47 Faggiano E, Fiorino C, Scalco E, Broggi S, Cattaneo M, Maggiulli E, et al., "An automatic contour propagation method to follow parotid gland deformation during head-and-neck cancer tomotherapy" *Phys Med Biol* **56**, 775-91 (2011).
- 850 48 ICRU. ICRU Report 62: Prescribing, Recording and Reporting Photon Beam Therapy. Bethesda, Md, USA: International Commission on Radiation Units and Measurements; 1999. Report No.: 62.
- 49 Rietzel E, Bert C, "Respiratory motion management in particle therapy" *Med Phys* **37**, 449-60 (2010).
- 50 Graeff C, Durante M, Bert C, "Motion mitigation in intensity modulated particle therapy by internal target volumes covering range changes" *Med Phys* (2012).
- 855 51 Ford EC, Mageras GS, Yorke E, Ling CC, "Respiration-correlated spiral CT: A method of measuring respiratory-induced anatomic motion for radiation treatment planning" *Med Phys* **30**, 88-97 (2003).
- 52 Rietzel E, Pan T, Chen GTY, "Four-dimensional computed tomography: Image formation and clinical protocol" *Med Phys* **32**, 874-89 (2005).
- 53 Lyons RG. *Understanding Digital Signal Processing*. 3 ed. Addison Wesley Pub Co Inc; 2010.
- 860 54 Frigo M, Johnson SG, "The design and implementation of FFTW3." *Proceedings of the IEEE* **93**, 216-31 (2005).
- 55 Furukawa T, Inaniwa T, Sato S, Shirai T, Mori S, Takeshita E, et al., "Moving target irradiation with fast rescanning and gating in particle therapy" *Med Phys* **37**, 4874-9 (2010).
- 56 Spielberger B, Krämer M, Scholz M, Kraft G, "Three-dimensional dose verification in complex particle radiation fields based on X-ray films" *Nucl Instrum Meth B* **209**, 277-82 (2003).
- 865 57 Karger CP, Jäkel O, Hartmann GH, "A system for three-dimensional dosimetric verification of treatment plans in intensity-modulated radiotherapy with heavy ions" *Med Phys* **26**, 2125-32 (1999).
- 58 Steidl P, Richter D, Schuy C, Schubert E, Haberer T, Durante M, et al., "A breathing thorax phantom with independently programmable 6D tumour motion for dosimetric measurements in radiation therapy" *Phys Med Biol* **57**, 2235-50 (2012).
- 870 59 Weber U, Kraft G, "Design and construction of a ripple filter for a smoothed depth dose distribution in conformal particle therapy" *Phys Med Biol* **44**, 2765-75 (1999).
- 60 Karger CP, Jäkel O, Palmans H, Kanai T, "Dosimetry for ion beam radiotherapy" *Phys Med Biol* **55**, R193-R234 (2010).
- 61 Puck TT, Marcus PI, "A rapid method for viable cell titration and clone production with HeLa cells in tissue culture: The use of X-irradiated cells to supply conditioning factors" *Proc Natl Acad Sci U S A* **41**, 432-7 (1955).
- 875 62 Krämer M, Durante M, "Ion beam transport calculations and treatment plans in particle therapy" *The European Physical Journal D* **60**, 195-202 (2010).
- 63 Elsässer T, Krämer M, Scholz M, "Accuracy of the local effect model for the prediction of biologic effects of carbon ion beams in vitro and in vivo" *Int J Radiat Oncol Biol Phys* **71**, 866-72 (2008).
- 880 64 Zhang X, Zhao KL, Guerrero TM, McGuire SE, Yaremko B, Komaki R, et al., "Four-dimensional computed tomography-based treatment planning for intensity-modulated radiation therapy and proton therapy for distal esophageal cancer" *Int J Radiat Oncol Biol Phys* **72**, 278-87 (2008).
- 65 Brock KK, "Results of a multi-institution deformable registration accuracy study (MIDRAS)" *Int J Radiat Oncol Biol Phys* **76**, 583-96 (2010).
- 66 Nohadani O, Seco J, Bortfeld T, "Motion management with phase-adapted 4D-optimization" *Phys Med Biol* **55**, 5189-202 (2010).

- 885 67 Unkelbach J, Bortfeld T, Martin BC, Soukup M, "Reducing the sensitivity of IMPT treatment plans to setup errors and range uncertainties via probabilistic treatment planning" *Med Phys* **36**, 149-63 (2009).
- 68 Haberer T, Becher W, Schardt D, Kraft G, "Magnetic scanning system for heavy ion therapy" *Nucl Instrum Meth A* **330**, 296-305 (1993).
- 890 69 Furukawa T, Noda K, Uesugi TH, Naruse T, Shibuya S. Intensity control in RF-knockout extraction for scanning irradiation. 2005 p. 32-5.
- 70 Schömers C, Feldmeier E, Haberer T, Naumann J, Panse R, Peters A. Implementation of an intensity feedback loop for an ion therapy synchrotron. 2011 p. 2851.
- 71 Sharp GC, Jiang SB, Shimizu S, Shirato H, "Prediction of respiratory tumour motion for real-time image-guided radiotherapy" *Phys Med Biol* **49**, 425-40 (2004).
- 895 72 Ruan D, Keall P, "Online prediction of respiratory motion: multidimensional processing with low-dimensional feature learning" *Phys Med Biol* **55**, 3011-25 (2010).
- 73 Siebenthal vM, Szekely G, Gamper U, Boesiger P, Lomax A, Cattin P, "4D MR imaging of respiratory organ motion and its variability" *Phys Med Biol* **52**, 1547-64 (2007).
- 74 Chen G, Sharp G, Mori S, "A review of image-guided radiotherapy" *Radiological Physics and Technology* **2**, 1-12 (2009).
- 900 75 Case RB, Moseley DJ, Sonke JJ, Eccles CL, Dinniwell RE, Kim J, et al., "Interfraction and intrafraction changes in amplitude of breathing motion in stereotactic liver radiotherapy" *Int J Radiat Oncol Biol Phys* **77**, 918-25 (2010).
- 76 Hild S, Durante M, Bert C, "Assessment of Uncertainties in Treatment Planning for Scanned Ion Beam Therapy of Moving Tumors" *Int J Radiat Oncol* (2012).

905